Surface Review and Letters, Vol. 3, No. 1 (1996) 263–280

ENERGETICS AND DYNAMICS OF MOLECULAR CLUSTERS

JOSHUA JORTNER, UZI EVEN, ALEXANDER GOLDBERG, and ISRAEL SCHEK
School of Chemistry, Tel Aviv University,
Ramat Aviv, 69978 Tel Aviv, Israel

TAMAR RAZ and RAPHAEL D. LEVINE
The Fritz Haber Research Center for Molecular Dynamics,
The Hebrew University of Jerusalem, Jerusalem 91904, Israel

We address some of the unique and basic features of molecular clusters, which involve (i) surface, interior, and site-selective energetics and dynamics, and (ii) the size dependence of the energetic, spectroscopic, electromagnetic, and dynamic attributes of large finite systems. Cluster-size equations provide a unified (but not universal) description of the "transition" of different attributes of clusters to those of the macroscopic bulk material. We explored fundamental issues, e.g., the physical origins of cluster-size effects, which originate either from cluster packing or from excluded volume contributions, and discussed some applications for the quantification of the size dependence of site-specific ionization potentials, extravalence and intravalence electronic spectroscopy, collective vibrational excitations, and dynamic effects. The quantification of dynamic cluster-size effects for energy acquisition in high-energy cluster-wall collisions opens avenues for the exploration of cluster-impact thermal femtosecond chemistry.

1. Prologue

We shall be concerned with the energetics and dynamics of molecular clusters,[1–3] i.e., finite aggregates containing $n = 2$–10^9 particles.[4–19] For some of us, trimers and tetramers (n=3,4) constitute an exciting research area, while others are fascinated by huge $(He)_n$ ($n \sim 10^6$) clusters,[20–28] e.g., excess electron binding in surface states of He clusters[29–32] with a localization onset at $n \gtrsim 3 \times 10^5$.[31,32] It was often stated[1–3] that cluster science builds bridges between molecular, surface, and condensed matter chemical physics. The broad scientific scope of the ISSPIC-7 clearly shows that these expectations have been fully realized. Furthermore, the central role of cluster chemical physics in bridging between scientific disciplines is of even broader scope and intrinsic significance. The exploration of the properties of large finite systems provides interrelationships between thermodynamics, atomic and nuclear physics, chemical binding, structure, condensed matter physics and chemistry, spectroscopy, molecular dynamics, and dynamics in the condensed phase.

Let us dwell first on the broad horizons of cluster chemical physics, ascending the "magic mountain" of the evolution of atomic, molecular, and condensed matter science during this century, by eight paths (Fig. 1). All eight paths go heavenward towards a unified and complete description of the structure–electronic level structure–energetics–dynamics interrelationships. Cluster science, whose modern conceptual framework was laid at the ISSPIC-1 in 1977,[4] builds a bridge between these eight paths (Fig. 1). According to Buddha[33] such a bridge constitutes a Middle Way, or rather an Eightfold Noble Way. Cluster science provides the Eightfold Noble Way between a broad spectrum of scientific disciplines.

Alluding to some of the historical perspectives of the development of cluster chemical physics, we realize that cluster science is quite old, originating at the beginning of the century with the work of Mie[34] on the optical properties of small particles, while the seminal work of Kubo[35] in 1962 laid the foundations for the understanding of the electronic properties of small metallic particles. A landmark in the study of clusters was provided in 1977 by Friedel[1] at the ISSPIC-1, by emphasizing the importance of the

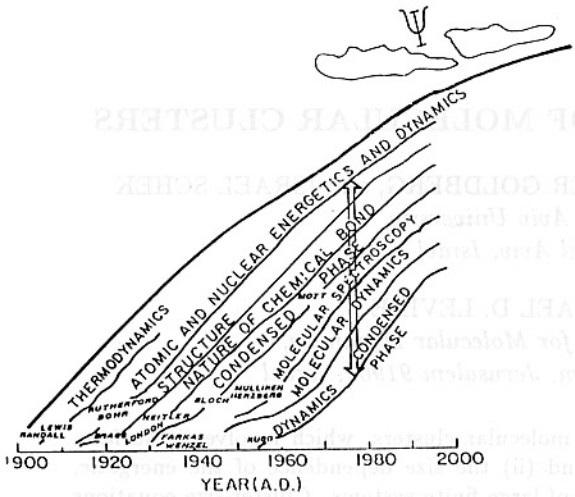

Fig. 1. An artist's view of the "magic mountain" of the evolution of atomic, molecular, and condensed matter science during this century. The clouds at the summit represent the unified and complete description of the structure – electronic level structure, energetic–dynamic interrelationships. Eight paths go to the peak. The names of some of the pioneers who initiated each scientific area are marked on the paths. The bridge between the eight paths (represented by an open arrow) was laid at the ISSPIC in 1977.

studies of "clean and isolated clusters", which at that time constituted a "theoretician's dream". The genesis of the chemical physics of isolated clusters originated from the following experimental and theoretical directions:

(A) The generation of cluster beams. In the 1960's Hagena, Gspann, and their colleagues[36–40] developed the experimental methods for the production and interrogation of cluster beams.

(B) Structural concepts. The conceptual framework for the field originated in the 1960's from structural considerations for the close packing of hard spheres in the icosahedral five-fold symmetry,[41] and the structural implications for rare-gas clusters.[42]

(C) Van der Waals molecules. The experimental[43–46] and theoretical[47,48] exploration of van der Waals molecules containing rare-gas atoms, laid the foundations for the elucidation of cluster structure, spectroscopy, and vibrational predissociation dynamics.

(D) Excess electron localization in supercritical polar fluids.[49–51] Spectroscopic studies of the localization of excess electrons in supercritical water and ammonia conducted in the 1970's (Refs. 49–51) could not be reconciled with the formation of an excess electron in a microscopically homogeneous medium, but rather invoked the concept of "the formation of a trapped electron localized in a cluster of polar molecules".[51] The direct experimental observation of hydrated electron $(H_2O)_n^-$ clusters was provided by Haberland and his colleagues about ten years later,[52–55] being followed by extensive experimental[56–65] and theoretical[29–32,66–76] work on internal[59–61,70–75,76] and surface[29–32,65,71–76] excess electron states in clusters.

The arsenal of experimental, computational, and theoretical methods for the exploration of clusters rests on the (partial catalogue) of the following approaches:

(i) Experimental methods.[4–19] These involve techniques for the production of cluster beams, structural determination, infrared and visible UV laser spectroscopy, synchrotron-radiation spectroscopy, photoelectron spectroscopy, mass-selection, near-threshold photoelectron and photon detection, electric polarizabilities, and magnetic moments, as well as cluster collisional processes with atoms, clusters and walls.

(ii) Simulations. These encompass classical molecular dynamics (MD) and Monte-Carlo simulations,[77–80] quantum path-integral MD calculations,[79,80] simulations of vibrational and electronic spectroscopic data,[81] and simulations of nonadiabatic dynamics.[82]

(iii) Quantum-mechanical computations. These pertain to density-functional methods,[83] atomic and nuclear physics techniques,[84,85] condensed matter models,[69] and advanced quantum-chemistry computations.[86–91]

Focusing on modeling and on theory, we note that both the simulations and the quantum-mechanical computations are intrinsically limited. The simulations mostly rest on the use of empirical pair potentials, whose accuracy cannot be readily assessed. On the other hand, the quantum-mechanical methods give the properties of the system at 0 K. The combination between quantum electronic calculations and

MD simulations is essential. The combination between density-functional electronic calculations and classical nuclear dynamics simulations was performed.[92–94] A most promising future trend will involve the merging between quantum-chemistry computations for the calculations of the many-body intermolecular forces and classical MD simulations of the nuclear motion. This *ab-initio* MD method is already implemented by Bonacic-Koutecky and her colleagues.[95]

This overview will focus on some novel aspects of molecular clusters:

1. Surface, interior, and site-selective spectroscopy.
2. Origins of cluster-size effects, which are due either to cluster packing or to excluded volume contributions.
3. Excluded volume effects on cluster ionization and excitation.
4. Collective cluster vibrational excitations.
5. The unified description of cluster-size effects.
6. Dynamic cluster-size effects.
7. Cluster-impact chemistry.

2. Surface, Interior, and Site-Selective Energetics and Dynamics

A unique characteristic of clusters pertains to their size-dependent large surface/volume ratio. The application of the celebrated liquid-drop model[96,97] to a cluster containing n constituents, gives for the fraction F of the surface constituents

$$F = \alpha n^{-1/3}, \qquad (1)$$

where α is a numerical constant, which is determined by the cluster shape (e.g., $\alpha = 4$ for a sphere). This coarse-grained, limiting relation should be extended in two directions for low-temperature, rigid, clusters. Firstly, quantitative information should be inferred for the structure and the energetics of distinct surface sites from detailed models and simulations for the packing of atomic and molecular clusters.[41,42,98–102] Secondly, the segregation between internal and surface sites provides only coarse-grained information. In this context, different energetic and spectroscopic observables will be exhibited for distinct sites in a neat cluster or for different substitutional sites of an impurity in a heterocluster.

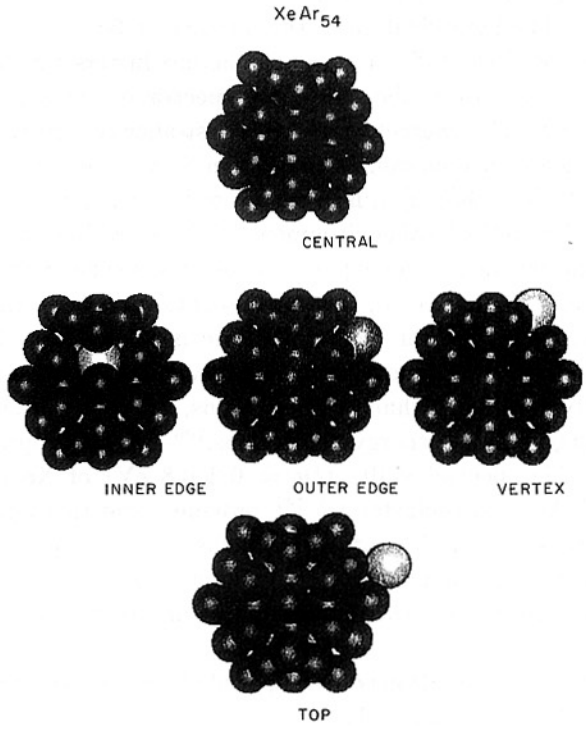

Fig. 2. Snapshots of the five distinct substitutional (C), (I), (O), (V), and (T) sites of Xe in $XeAr_{54}$.

To demonstrate the structural implications of distinct surface sites and of different interior sites in a rigid cluster, we consider the structures (obtained by the conjugate gradient quenching[103,104] of the $XeAr_{54}$ heterocluster (Fig. 2). The ground-state substitutional Xe atom configurations are:[41,42] (C) central position, (I) inner edge, (O) outer edge, and (V) vertex (Fig. 2). In addition, the (T) top Xe atom absorbed on the cluster surface (Fig. 2) was studied. The (O), (V), and (T) sites correspond to distinct surface states, while the (C) and (I) sites represent different interior configurations. MD simulations reveal several interesting temperature-induced configurational changes in $XeAr_n$ heteroclusters:[105] (a) A ground-state configurational dilation around the (C) site, which is manifested by the increase of the (average) nearest-neighbor Xe–Ar distance, the increase in the number of nearest neighbors and a motion of the Xe atom off-center. This configurational change is exhibited at $T = 13$ K for $n = 54$ and $T_c = 37$ K at $n = 146$. (b) Surface melting, which is manifested by the diving of the (T) atom into the first cluster shell, being exhibited at $T_{SM} \gtrsim 25$ K for $n = 54$ and

$T_{SM} \simeq 35$ K for $n = 146$.

The identification of the distinct surface and interior sites in $XeAr_n$ rare-gas heteroclusters can be obtained from the electronic spectra of the guest atom. The energetics of the lowest-allowed extravalence electronic excitation of Xe in $XeAr_n$, i.e., $^1S_0 \rightarrow {}^3P_1(^2P_{3/2}6s[3/2]_1)$, is expected to be extremely sensitive to the local environment,[106–116] providing ways and means for the exploration of site-specific excitations. The spectral shift in absorption of Xe in the elemental cluster (relative to the isolated atom) is dominated by short-range repulsive non-orthogonality overlap–exchange interactions, which result in large positive energy corrections.[106–116] The appreciable spectral shifts ($\delta\nu = 0.2$–0.8 eV) of Xe in $XeAr_n$ heteroclusters[137–141] provide a spectroscopic probe for the identification of distinct surface configurations of a guest atom and for the spectroscopic interrogation of the atomic shell structure in rare-gas clusters.

The simulations of the optical absorption spectra rest on two approaches:

(i) The evaluation of the first and second spectral moments of the absorption line shape.[117–120] These observables are calculated from the time-dependent energy gap

$$U(t) = V_e(t) - V_g(t)\,, \tag{2}$$

where $V_g(t)$ and $V_e(t)$ are the ground and excited state potential energies at time t, respectively. The first and second moments M_1 and M_2, respectively, of the energy gap are

$$M_1 = \langle U(t)\rangle\,, \tag{3}$$

and

$$M_2 = \langle U(t)^2\rangle\,. \tag{4}$$

These classical expressions for the first and second moments are identical to the quantum results. The spectral shift $\delta\nu$ (relative to the bare atom) is well represented by the first moment

$$\delta\nu = M_1\,. \tag{5}$$

In the Kubo slow modulation limit[121] the line shape is Gaussian with the spectral linewidth (FWHM) Γ being determined by the weighted second moment

$$\Delta^2 = M_2 - M_1^2\,, \tag{6}$$

in the form $\Gamma = \eta\Delta$ where $\eta = 2.355$.

(ii) The semiclassical spectral density method,[81,121–136] which allows for the calculation of the entire line shape $L(E)$, is given by

$$\begin{aligned} L(E) &= (1/\pi)\mathrm{Re}\int_\Omega dpdq\,\rho(p,q)\int_0^\infty d\tau \\ &\quad\times \exp[i(E-\omega_{eg}-\langle U\rangle)\tau] \\ &\quad\times \exp[-g(\tau,p,q)]\,, \end{aligned} \tag{7}$$

where E is the photon energy, ω_{eg} is the energy gap of the bare atom, $g(\tau,p,q)$ is the two-time integral of the semiclassical energy-gap autocorrelation function in the time domain, $\rho(p,q)$ represents the distribution function of the ground electric state in the accesible region (Ω) of the phase space, while p and q are the momenta and coordinates of the atoms, respectively.

The semiclassical method, Eq. (7), was applied to simulate the absorption spectra of $XeAr_N$ clusters,[105] using as input data reliable excited state $Xe(^3P_1)$–$Ar(^1S_0)$ pair potentials, adopted from the work of Messing, Raz, and Jortner.[113,114] The size dependence of the absorption spectra for the central (C) site ($N = 12$–199) portrayed in Fig. 3 reveals Gaussian line shapes, which, according to the analysis of their power spectra,[105] correspond to the Kubo slow modulation limit,[121] with the linewidth and spectral shift given by Eqs. (5) and (6). The spectral shifts

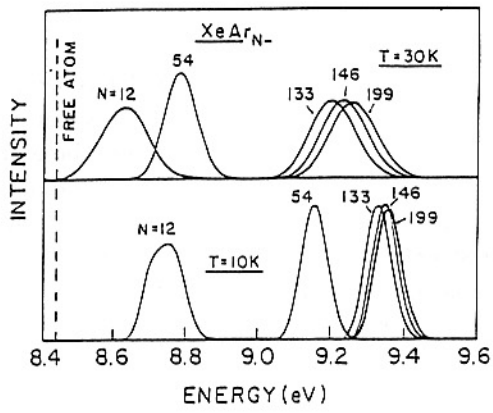

Fig. 3. Cluster size and temperature dependence of the line shapes for the central (C) Xe substitutional site. The dashed vertical line represents the bare Xe atom excitation.

for lower ($N = 12, 54$) clusters reveal strong temperature dependence (Fig. 3) due to ground-state configurational relaxation, while for large clusters ($N = 133$–199) $\delta\nu$ assume large values (0.80–0.83 at 30 K).

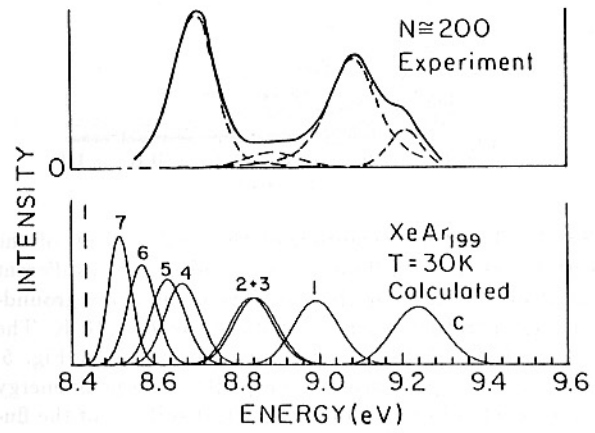

Fig. 4. The comparison between the calculated site-specific line shapes of $XeAr_{199}$ at $T = 30$ K (lower panel) and the experimental spectrum (Ref. 139) of $XeAr_{200}$ prepared in a supersonic expansion of 0.01%Xe+Ar (upper panel). The calculated line shapes are labeled by the specific sites: C=center site, 1–4 interior sites, and 5–8 substitutional surface sites. The experimental spectrum is decomposed into separate (dashed line) Gaussians, which represent site-specific excitations (Ref. 139). The vertical dashed line is the bare Xe atom excitation.

Möller and his colleagues[137–141] applied energy- and time-resolved fluorescence methods with synchrotron-radiation excitation to study excited state energetics and dynamics of the $^1S_0 \rightarrow {}^3P_1$ excitation of Xe in $XeAr_N$ ($N = 1$–5000). Our simulations (for $N = 12$–206) at $T = 30$–35 K,[105] will be confronted with the experimental reality.[137–141] The experimental highest absorption band in moderately large $XeAr_N$ ($N = 200$) clusters ($\delta\nu = 0.78$ eV) is well accounted for (Fig. 4) in terms of simulation for the excitation of (C) site. In Fig. 4 we display the simulated site-specific absorption bands for the interior sites (1)–(4) and the surface sites (5)–(7) of $XeAr_{199}$ at $T = 30$ K, together with the experimental spectrum of $XeAr_{200}$ [prepared in a Xe(0.01%) + Ar supersonic expansion].[139–141] The experimental band at $\delta\nu = 0.27$ eV (Fig. 4) is assigned to substitutional surface sites (4)–(6), with the linewidth containing inhomogeneous contributions. The experimental band at $\delta\nu = 0.66$ eV and the broad band $\delta\nu = 0.46$ eV in $XeAr_{200}$ (Fig. 4) are assigned to interior sites, i.e., (1) and (2) sites, respectively. This spectroscopy assignment provides an overview of site-specific impurity excitations. Selective spectroscopy of surface states was obtained from (Xe+Ar_N) crossed beam experiments.[139–141] A remarkable feature of the experimental spectrum of $XeAr_{150}$ prepared in crossed beams[140,141] (Fig. 5) is the "spectroscopic desert" in the range 8.8–9.4 eV, whereupon the contributions of the (C) site and of the interior (1), (2), and (3) sites are negligible. The prominent experimental absorption band, which peaks at 8.7 eV, is assigned to the superposition of the excitations of the Xe substitutional surface sites (4), (5), and (6), with a major contribution from the surface site (4) (Fig. 5). The experimental linewidth $\Gamma = 0.12$ eV exceeds the calculated linewidth ($\Gamma = 0.10$ eV at $T = 30$ K), presumably reflecting inhomogeneous broadening. Finally, we note that the excitation of the (T) top atom is missing, being precluded by surface melting.

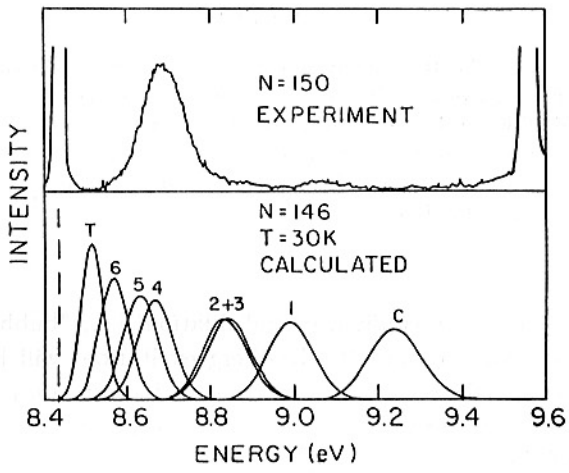

Fig. 5. The comparison between the calculated site-specific line shapes of $XeAr_{146}$ at $T = 30$ K (lower panel) and the experimental spectrum of $XeAr_{150}$ prepared in a crossed beam experiment of Xe+Ar_N (Refs. 140 and 141). The calculated line shapes are labeled by the specific sites (C)–central Xe substitutional site, (1)–(3) interior Xe substitutional site, (4)–(6) surface Xe substitutional sites, and (T)–top site. The horizontal dashed line is the bare Xe atom excitation.

The information on the energetics, manifested by $\delta\nu$, and on the nuclear dynamics, emerging from the homogeneous line shape, provides the basis for the exploration of excited state dynamics. Of considerable interest is the dynamics of configurational nuclear relaxation around electronic extravalence excitations.[142] Figure 6 portrays the time evolution of the average Xe–Ar nearest-neighbor distance R_{NN} in $XeAr_{146}$, following the excitation of the (C) site. The configuration dilation occurs on a time scale of 300–500 fsec, being manifested by the marked increase of R_{NN}.

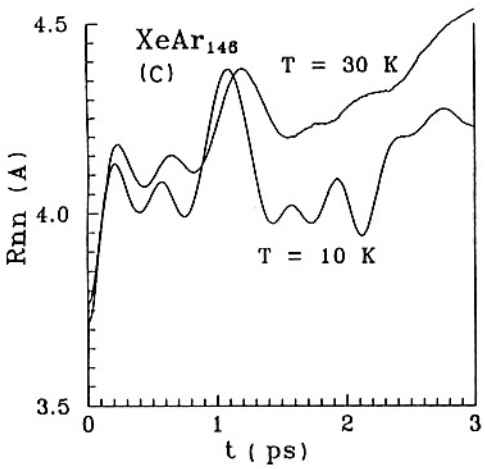

Fig. 6. The time evolution of the average Xe–Ar distance R_{NN} of Xe ($^3P_1$) at the (C) site in $XeAr_{146}$. $T = 10$ and 30 K mark the equilibrium ground-state cluster temperatures prior to excitation. Note the configuration dilution manifested by the increase of R_{NN} on the time scale of $\sim$ 300 fsec.

This large configurational dilation, i.e., "bubble formation" around the Rydberg excitation, will be manifested in a small spectral shift in emission relative to the free-atom energy and in a large Stokes shift between the absorption and the emission peak energies. The simulated temporal evolution of the fluorescence peak from the (C) site (Fig. 7) reveals a dramatic decrease from the initial value of $\delta\nu = 0.8$ eV to $\delta\nu \simeq 0.08$ eV at $t = 1$ psec. In Fig. 7 we also show the implications of site-specific excited state nuclear dynamics for the excitation of different Xe sites of $XeAr_{146}$. The configurational relaxation times for the interior sites (1)–(3) and for the surface

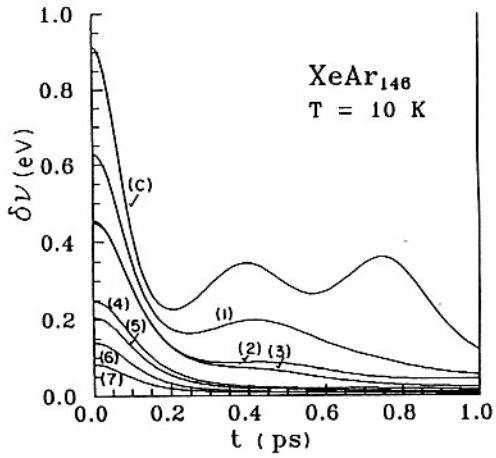

Fig. 7. The time evolution of the peak energy of the $Xe(^3P_1) \rightarrow Xe(^1S_0)$ fluorescence band of Xe in different initial sites in $XeAr_{146}$ clusters. The equilibrium ground-state temperature prior to excitation is $T = 10$ K. The specific (C), (1)–(6) Xe sites are labeled as in Fig. 5, with site (7) representing the top site. The peak energy is represented in terms of the spectral shift $\delta\nu$ of the fluorescence maximum relative to the bare-atom excitation.

sites (4)–(6) and (7) are $\sim$ 100–200 fs (Fig. 7). The complete time evolution of $\delta\nu$ in emission for different sites occurs on a time scale of $\sim$ 1 psec, with $\delta\nu$ converging to low (0.08–0.02 eV) values. As the radiative lifetime of the $Xe(^3P_1)$ state is on the nsec time domain, the time evolution of $\delta\nu$ contributes 0.1% to the fluorescence yield. Nevertheless these dramatic sub-picosecond dynamic effects may be amenable to experimental observation either by upconversion fluorescence or by time-resolved absorption studies.

3. Origins of Cluster-Size Effects

A key concept for the quantification of the unique characteristics of atomic and molecular clusters pertains to size effects.[143–146] These involve the evolution of structural, thermodynamic, electronic, energetic, electromagnetic, dynamic, and chemical features of finite systems with increasing the cluster size. Cluster-size effects fall into two distinct domains:

(A) Specific size effects. In the "small cluster" size domain an irregular size dependence of the relevant cluster properties $\chi(n)$ (where n is the number of constituents) is exhibited. This ir-

regular pattern is manifested most dramatically in the existence of "magic numbers" in $\chi(n)$ vs n, which reflect shell-closure effects. Typical examples involve the structural closed shells of Mackay icosahedra[41,42] in clusters of rare-gas atoms[98–102] and of spherical large molecules,[103] the enhanced energetic stability and the increased ionization potentials for electronic closed shells in metal clusters,[84,85] and the expected increased stability of the Fermion closed shell structure in $(^3He)_N$ clusters.[147–149]

(B) Smooth size effects, which are revealed for "large" clusters. In this size domain a quantitative description was advanced for the "transition" of energetic, electronic, spectroscopic, electrodynamic, and dynamic attributes of clusters to the infinite bulk system in terms of cluster-size equations (CSEs),[143–146]

$$\chi(n) = \chi(\infty) + An^{-\beta}, \tag{8}$$

where A is the constant and $\beta(\beta \geq 0)$ is a positive exponent.

CSEs, which are quantified by Eq. (8), can be traced to two distinct physical origins: cluster packing and excluded volume effects. These two categories will now be considered.

3.1. *Size effects originating from cluster packing*

These effects pertain to the consequences of the large surface/volume fraction of clusters. For sufficiently large clusters, the fraction of the surface atoms is given by Eq. (1). A straightforward utilization of this result pertains to the description of extensive variables Y, e.g., the internal energy, entropy, or magnetization of the cluster. Viewing the cluster of n constituents as a composite system consisting of surface and volume subsystems, the value of the extension variable $Y(n)$ is obtained from an additivity rule for these subsystems

$$Y(n) = n(1-F)y_v + nFy_s, \tag{9}$$

where y_v and y_s are the corresponding variables (per constituent) for the bulk and surface, respectively. The total value of the variable per constituent $y(n) = Y(n)/n$ is obtained from Eqs. (1) and (9) in the form

$$y(n) = y_v + \alpha(y_s - y_v)n^{-1/3}. \tag{10}$$

Equation (10) constitutes a simple application of the liquid-drop model,[96,97] which was advanced in nuclear physics. Equation (10) is isomorphous to the CSE, Eq. (8).

A useful application of the CSE, Eq. (10), due to cluster packing, involves the description of the internal energy per constituent $u(n) = U(n)/n$ of the cluster of total internal energy n, which can be described in the form

$$u(n) = u_v + \alpha(u_s - u_v)n^{-1/3}, \tag{11}$$

where u_v and u_s are the energy (per constituent) for the volume and surface constituents, respectively.[143,150,151]

3.2. *Size effects originating from excluded volume contributions*

A multitude of energetic and spectroscopic size effects can be described in terms of the infinite system observable, which is corrected to the excluded volume contribution. The CSE, Eq. (8), then assumes the general form

$$\chi(n) = \chi(\infty) + C(n), \tag{12}$$

where

$$C(n) = An^{-\beta} \tag{13}$$

is the excluded volume correction term. $C(n)$ accounts for the modification of the bulk value for the observable in the cluster, due to the excluded volume outside it (i.e., the range R_c to ∞). R_c is the cluster radius, which is related to the radius R_0 of a single constituent by

$$R_c = R_0 n^{1/3}. \tag{14}$$

Accordingly, the excluded volume correction can be expressed in the alternative form

$$C(R_c) = A(R_c/R_0)^{-3\beta}. \tag{15}$$

As was previously pointed out,[143] the CSE, Eq. (12), is better than it appears at first sight for the quantification of the physical observables. All the short-range contributions to $\chi(n)$, which are usually difficult to evaluate, are incorporated in $\chi(\infty)$, which is often taken from experiment. What is explicitly evaluated is the correction term $C(n)$ arising from the excluded volume contributions. These excluded volume contributions are determined by long-range

effects, which are amenable to a reliable calculation. We shall now apply excluded volume effects to the energetics and spectroscopy of clusters.

4. Excluded Volume Effects on Cluster Ionization and Excitation Energetics

The CSE, Eq. (12), was successfully applied to a multitude of energetic and spectroscopic size effects.[143–146] Some relevant examples are listed below.

4.1. *Charging energy contributions to cluster ionization potentials*

Here $C(n)$, Eqs. (13) or (15), originates from the charging energy contributions to the cluster ionization potential. For the creation or removal of a charge from the center of a spherical cluster, the application of the continuum dielectric model for the excluded volume outside the cluster results in $C(R_c) \propto R_c^{-1}$, so that $C(n)$ is given by Eq. (13) with $\beta = 1/3$. This situation is realized for the vertical ionization potentials of rare-gas clusters, the ionization potentials of metal clusters,[143] and the vertical binding energies of interior excess electron states in large $(NH_3)_n^-$ clusters.[57] The excluded volume contribution of an impurity in a heterocluster depends on the location of the impurity. The distribution between surface and interior impurity states is of interest in the context of anion solvation in water clusters, e.g., $X^-(H_2O)_n$ ($X = F, C\ell, Br, I$)[88–91, 152–160] and of rare-gas heteroclusters (Sec. 2).[105,137–141] The dielectric model[161–165] for the surface configurations results in the excluded volume correction to the ionization potential of the form $C(R_c) \propto R_c^{-1}[1 + f(R_c^{-1})]$, where $f(\cdot)$ is a small correction function.[165] The ionization potentials of distinct sites in a neat cluster or a heterocluster are different and a theory of site-specific cluster ionization potentials was recently developed.[165]

4.2. *Electronic heterocluster spectroscopy*

Optical absorption spectra of $M \cdot A_n$ heteroclusters, consisting of an aromatic molecule (M) embedded in a cluster of inert-gas atoms (A) which correspond to an intravalence excitation of M, are of interest in relation to the microscopic interrogation of solvation phenomena, and for the utilization of M as a probe for the cluster microenvironment and nuclear dynamics.[119,120,129,130,166–174] The cluster-size dependence of the electronic excitations, i.e., the spectral line shapes, their spectral shifts $\delta\nu$, Eqs. (3) and (5), and their weighted second central moments Δ^2, Eq. (6), can be quantified in terms of CSEs. The CSEs for the optical properties rest on a spherical representation of the cluster with the impurity being located at an interior central configuration. The spectral shifts are due to cumulative M–A dispersive interactions, while the second moment originates from short-range nuclear dynamic effects.

The spectroscopic observables, $\delta\nu$ and Δ, are determined by integrals of the powers of the product $e(\mathbf{r})g(\mathbf{r})$ over the cluster volume, where $g(\mathbf{r})$ represents the isotropic radial distribution function and $e(\mathbf{r})$ corresponds to the microscopic (dispersive) spectral shift exerted on M by a single atom located at $\mathbf{r}$. We express the two lowest spectral moments $M_1(R_c)$ and $\Delta(R_c)$ of the cluster in terms of the moments $M_1(\infty)$ and $\Delta(\infty)$ of the bulk system, which are corrected to the contribution of the excluded volume[144]

$$M_1(R_c) = M_1(\infty) - C_1(R_c)\,, \tag{16}$$

and

$$[\Delta(R_c)]^2 = [\Delta(\infty)]^2 - C_2(R_c)\,, \tag{17}$$

where the excluded volume corrections are

$$C_1(R_c) = \bar{\rho}\int_{R_c}^{\infty} d^3\mathbf{r}\; e(\mathbf{r})\; g(\mathbf{r})\,, \tag{18}$$

$$C_2(R_c) = \bar{\xi}\int_{R_c}^{\infty} d^3\mathbf{r}\; [e(\mathbf{r})\; g(\mathbf{r})]^2\,, \tag{19}$$

where $\bar{\rho}$ is the average density and $\bar{\xi} = \bar{\rho}^2 k_B T \kappa_T$, where κ_T is the isothermal compressibility.

As usual, we consider a sufficiently large cluster (with $R_c \gg R_M > R_0$, where R_M is the average radius of M), where the excluded volume ($r \geq R_c$) is microscopically homogeneous, i.e., $g(\mathbf{r}) = 1$. The microscopic dispersive spectral shifts exerted by the atoms in the excluded region can be taken as isotopic in their asymptotic form $e(r) = -\gamma/r^6$. Equations (18) and (19) for an $M \cdot A_n$ heterocluster then result in the correction to M_1: $C_1(R_c) = \bar{A}_1 R_c^{-3} = A_1 n^{-1}$, where $\bar{A}_1 = -4\pi\gamma\bar{\rho}/3 = -\gamma R_0^{-3}$ and $A_1 = -\gamma R_0^6$. For the correction to Δ we get $C_2(R_c) = \bar{A}_2 R_c^{-9} = A_2 n^{-3}$, where $\bar{A}_2 = 4\pi\bar{\xi}\gamma^2/9$ and $A_2 = (4\pi\bar{\xi}\gamma^2/9)R_0^{-9}$.

The CSE for the spectral shift is

$$\delta\nu(n) = \delta\nu(\infty) + A_1 n^{-1}, \qquad (20)$$

where $A_1 = \gamma/R_0^6$. The linewidths are determined by Δ, which exhibits the CSE

$$\Delta(n) = \Delta(\infty) - \bar{B} n^{-3}, \qquad (21)$$

where $\bar{B} = A_2/2\Delta(\infty)$. In the fast modulation limit ($\tau_c\Delta/\hbar < 1$) the homogeneous spectral linewidth $\Gamma_f = 2\Delta^2\tau_c/h$ (i.e., the dephasing width) is

$$\Gamma_f(n) = \Gamma_f(\infty) - (2A_2\tau_c/\hbar)n^{-3}, \qquad (22)$$

where τ_c is decay time for the energy-gap autocorrelation function.

For the slow modulation limit ($\tau_c\Delta/\hbar > 1$) the linewidth $\Gamma_s = \eta\Delta$ (with $\eta = 2.355$) is

$$\Gamma_s(n) = \Gamma_s(\infty) - Bn^{-3}, \qquad (23)$$

where $B = \eta A_2/2\Delta(\infty)$. Equation (23) for the slow modulation is useful for large clusters, with the parameter B appearing in this limit being $B = [k_B T\kappa_T/8\pi R_0^3\Delta(\infty)]$.

The CSEs for $\delta\nu(n)$ and for $\Gamma(n)$ imply that the size dependence of the two spectroscopic observables is different, providing a specific example for the nonuniversality of the CSEs. The test of the CSEs, Eqs. (20) and (23), is provided by experimental data[120] and MD simulations[120] for $\delta\nu(n)$, and by MD simulations for 9-10-dichloroanthracene (DCA)-inert-gas heteroclusters. In Fig. 8 we portray the size dependence of $\delta\nu(n)$ and $\Gamma_s(n)$ for DCA·Kr_n (n = 5–28) heteroclusters. The increase of $|\delta\nu(n)|$ with increasing n is well accounted for by Eq. (20), while the weak size dependence of $\Gamma_s(n)$ is qualitatively consistent with the predictions of Eq. (23). To provide a quantification of the spectroscopic CSEs we present in Fig. 9 the experimental data for the size dependence of the spectral shifts of DCA·Ar_n (n = 1–55) heteroclusters, together with the results of MD simulations of this observable,[120] which are in excellent agreement with the experimental data. In the size domain n = 30–55, $\delta\nu(n)$ exhibits a monotonous, although pronounced, size dependence which is consistent with Eq. (20) with $\delta\nu(\infty) = -610$ cm^{-1}. In the insert to Fig. 9 we analyzed the available experimental data for the cluster-size dependence of $\delta\nu(n)$ for DCA·Ar_n with n = 30–55,[120] for $n = 1000 \pm 500$,[175] and for $n = \infty$ (i.e., the Ar matrix spectrum; Ref. 176). These experimental data follow the linear relationship $\delta\nu(n)/\text{cm}^{-1} = -610 + 4.2 \times 10^3 n^{-1}$, in

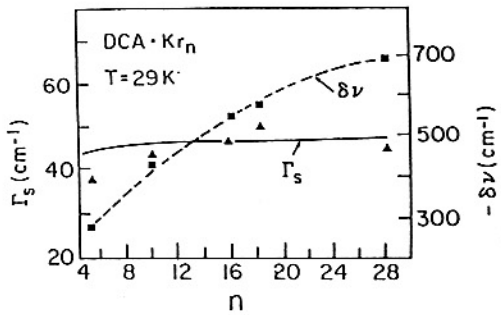

Fig. 8. MD simulations of the spectral shifts $\delta\nu$ (■) and of the homogeneous linewidths, $\Gamma_s = \eta\Delta$ (▲) for the large DCA·Kr_n (n = 5–28) clusters at 29 K according to Refs. 120 and 144. The MD simulation results were fitted by the CSEs for these observables. The dashed line represents the CSE for $\delta\nu$, Eq. (20), with $\delta\nu(\infty) = -900$ cm^{-1} and $A = 5.6 \times 10^3$ cm^{-1}. The solid line represents the CSE for Δ, Eq. (23), with $\Delta(\infty) = 45$ cm^{-1} and $B = 40$ cm^{-1}.

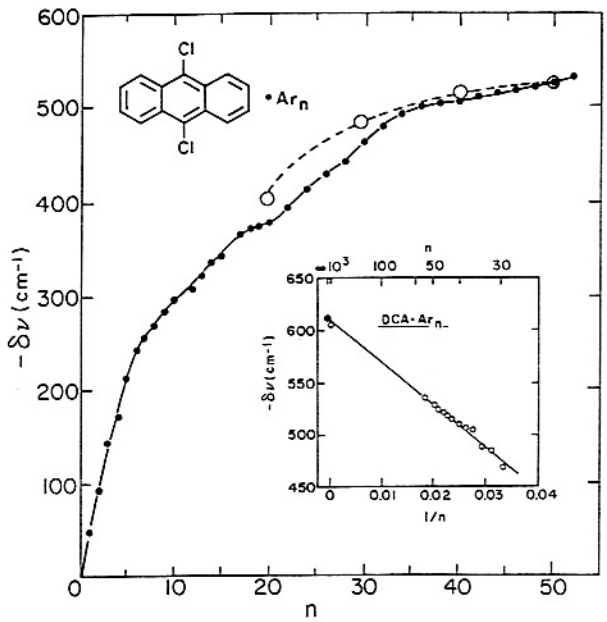

Fig. 9. The size dependence of the experimental $\delta\nu$ data for DCA·Ar_n (n = 1–55) clusters from Ref. 120 (• and solid curve). For large clusters $\delta\nu$ is accounted for by the CSE, Eq. (20), presented by open circles (○ and dashed curve). The insert shows the CSE for these experimental $\delta\nu$ data for n = 30–55 (Ref. 120), $n = 1000 \pm 500$ (Ref. 175), and the bulk solid (Ref. 176), which display the linear relation of $\delta\nu$ vs n^{-1}, according to Eq. (20).

accord with the CSE for $\delta\nu(n)$, Eq. (20). The beauty of this analysis is in transcendenting computer simulations and providing analytic results for the analysis of spectroscopic data.

5. Bulk and Surface Collective Vibrational Modes

An interesting example of size effects, originating from cluster packing, are surface collective vibrational modes and interior compression modes.[96,97] The collective cluster excitations can be treated by the application of the nuclear physics liquid-drop model.[96,97] The frequencies of surface collective modes are[24,96,97,145,146]

$$\hbar\omega_s(n) = an^{-1/2}, \tag{24}$$

where $a = [\ell(\ell-1)(\ell+2)A_s/3\mu R_0^2]$. Here ℓ is the angular momentum quantum number, A_s the surface energy, and R_0 is the radius of a single constituent of mass μ. The frequency of the interior mode of compression breathing is[24,96,97,145,146]

$$\hbar\omega_b(n) = bn^{-1/3}, \tag{25}$$

where $b = \pi\hbar c/R_0$ and c is the velocity of sound. The distinct size dependence of $\hbar\omega_s(n)$ and $\hbar\omega_b(n)$ originates from the different dispersion laws for surface riplons $[\omega(q) \propto q^{3/2}]$ and for bulk compression excitations $[\Omega(q) \propto q]$. Note that for these vibrational modes for the liquid (nonrigid) cluster $\hbar\omega_s(\infty) = \hbar\omega_b(\infty) = 0$. For a rigid (solid) cluster the interior compression mode, Eq. (25), has to be modified to include the contribution $\hbar\omega_b(\infty)$ of the surface phonons of the infinite solid, resulting in the CSE

$$\hbar\omega_b(n) = \hbar\omega_b(\infty) + bn^{-1/3}. \tag{26}$$

Vibrational collective excitations of $(^4\mathrm{He})_n$ and $(^3\mathrm{He})_n$ clusters, which are liquid down to 0 K[22-24] were calculated,[24,145,146] resulting in $\hbar\omega_b(n) = 25.6n^{-1/3}$ K for $(^4\mathrm{He})_n$ (Fig. 10) and $\hbar\omega_b(n) = 17.9^{-1/3}$ K for $(^3\mathrm{He})_N$ (Fig. 11). For the quadrupole ($\ell = 2$) surface modes of $(^4\mathrm{He})_n$ the collective vibrational excitations are[24,145,146] $\hbar\omega_s(n) = 10.5n^{-1/2}$ K (Fig. 10).

No direct experimental observations of these collective vibrational excitations for $(\mathrm{He})_n$ clusters are yet available. On the experimental front, some interesting expectations can be provided. The binding

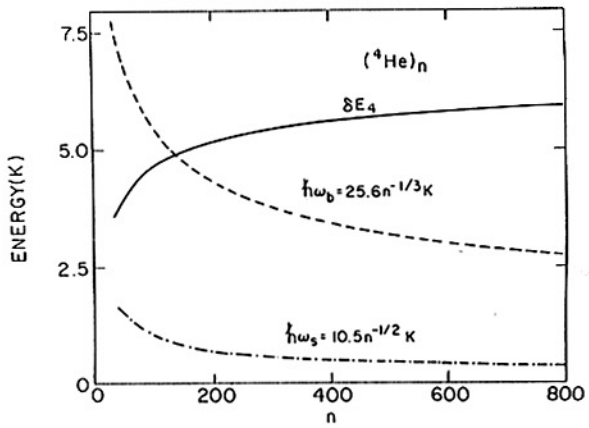

Fig. 10. Cluster-size dependence of the energies of the surface ($\hbar\omega_s$) and interior compression ($\hbar\omega_b$) collective vibrational modes of $(^4\mathrm{He})_n$ clusters. The CSEs, Eqs. (24) and (25) are obeyed. δE_4 is the binding energy per atom.

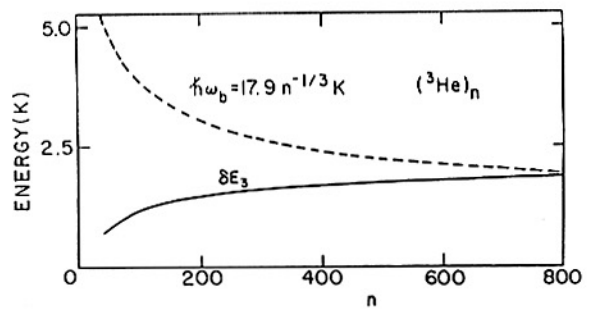

Fig. 11. Cluster-size dependence of the energy of interior compression collective vibrational mode of $(^3\mathrm{He})_n$ clusters, as calculated from Eq. (25). δE_3 is the binding energy per atom.

energies per atom δE_4 for $(^4\mathrm{He})_n$ and δE_3 for $(^3\mathrm{He})_n$ are smaller than the frequency of the interior mode for relatively small clusters, i.e., $\delta E_4 < \hbar\omega_b(n)$ for $n < 180$ and $\delta E_3 < \hbar\omega_b(n)$ for $n < 800$ (Figs. 10 and 11). In this cluster size domain one-quantum-induced evaporation of $^4\mathrm{He}$ or $^3\mathrm{He}$ atoms from the cluster will occur. The size onset for this single-atom evaporation will exhibit a striking isotope effect. The quadrupole surface collective vibrational frequencies are too low relative to δE_4 (Fig. 10) to induce a one-quantum evaporation. A more isoteric implication of these collective vibrational modes pertains to their coupling to electronic states of an excess electron on the surface of a large $(\mathrm{He})_n$ cluster.[31] These bound surface excess electron states constitute

Table I. Estimates of "critical" cluster sizes for the attainment of bulk properties.

Observable	β	n_-^a	$\lvert A/\chi(\infty)\rvert$	n_c^b
Cohesion energy alkali clusters	1/3	5	1	10^6
Ionization potentials of rare-gas clusters	1/3	20	0.1	10^3
Ionization potentials and electron affinities of metal clusters	1/3	60	0.7	3×10^5
Photoionization of $I^-(H_2O)_n$	1/3	125	1	10^6
Photoionization of $(NH_3)_n^-$	1/3	150	3	3×10^7
Collective vibrational compression modes of Ar_n	1/3	20	5	10^8
Confined Wannier excitons in rare-gas clusters	2/3	700	1	10^3
Dispersive spectral shift $M \cdot A_n$ cluster	1	10	7	7×10^2
Dispersive spectral width $M \cdot A_n$ cluster	3	10	1	7

[a] Rough estimates for the minimal cluster size ($n > n_-$) for the applicability of the CSE. Reference 143 in present work.
[b] Relative deviation of physical property from bulk value $\leq 1\%$.

giant electronic states with weak (ground state) binding energies,[30,31] $E_{1,0}$, i.e., -0.695 meV $\leq E_{1,0} \leq 0$, which raise interesting questions regarding the separation of electronic and nuclear motion in these systems. For large clusters in the size domain $n \simeq 10^6$, $E_{10} \simeq -0.26$ K and the electronic energy is comparable to the vibrational interior collective mode ($\hbar\omega_b \simeq 0.26$ K). Under these extraordinary circumstances the conventional Born–Oppenheimer separability between electronic and nuclear motion may break down.

A beautiful experimental verification of the existence of the cluster compression breathing mode was obtained by Buck and Krohne[177] from scattering of He atoms from Ar_n (n = 25–4600) clusters. The cluster-size dependence of the maximum of the vibrational energy transfer obeys the CSE, Eq. (26), with the intercept $\hbar\omega_b(\infty)$ being given by the Rayleigh mode of the (001) surface phonons of bulk solid Ar.

6. The Unified Description of Cluster-Size Effects

The description of "smooth" cluster-size effects [in range (B)], which originate either from cluster packing or from excluded volume contributions, results in the quantification of the gradual "transition" from the large finite cluster to the bulk systems. The CSE, Eq. (8), provides a unified description for the energetic, quantum, electronic, spectroscopic, and electrodynamic size effects.[143–146] Table I provides an overview of the parameters of CSEs for a multitude of physical attributes, which are specified in terms of the β exponent. Table I also shows the validity conditions for the applicability range of these CSEs, which are specified in terms of the minimal number n_- of constituents for the onset of range (B). From the data in Table I, i.e., distinct CSEs (with different values of β and n_-) for different physical properties, it is apparent that the cluster-size effects are not universal.

The CSEs provide the first quantitative answer to one of the central questions in the area of cluster chemical physics.[3,143] What is the minimal cluster size for which the cluster properties become size invariant and do not differ in any significant way from those of a macroscopic sample of the same material? According to the CSE, the relative deviation from the bulk value for a specific physical property $\chi(n)$ will be

$$|\chi(n) - \chi(\infty)|/|\chi(\infty)| = |A/\chi(\infty)|n^{-\beta}. \quad (27)$$

Defining somewhat arbitarily the realization of bulk properties for $n \geq n_c$ when the relative deviation is $\leq 1\%$, one estimates for the number of constituents, n_c, the "critical" cluster size to be

$$n_c = 100^{1/\beta}|A/\chi(\infty)|^{1/\beta}. \quad (28)$$

Table I provides a compilation of the values of $|A/\chi(\infty)|$. The catalogue of n_c (Fig. 12) reveals a variation of n_c over eight orders of magnitude for various physical properties. The largest value of n_c corresponds to electromagnetic interactions (e.g., the Einstein coefficients for spontaneous and stimulated emission) which are characterized by the dimensionless size parameter $(2\pi R_0/\lambda)n^{1/3}$, where λ is the wavelength of light.[143] On the other extreme, dispersion interactions result in the lowest values of n_c. From the foregoing analysis we conclude that the CSEs provide an unified (but not universal) description for the merging between the properties of microscopic large finite systems and those of the macroscopic bulk material.

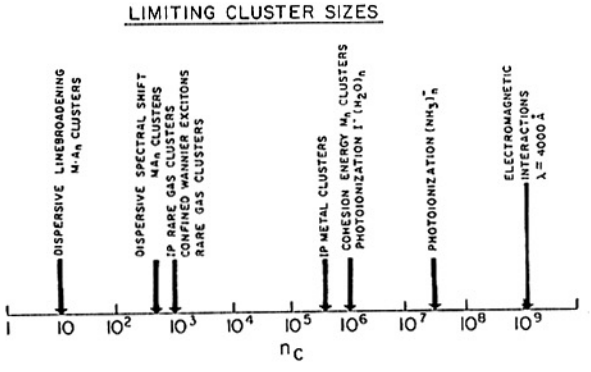

Fig. 12. An overview of the critical cluster size (n_c) for the attainment of bulk properties for different observables.

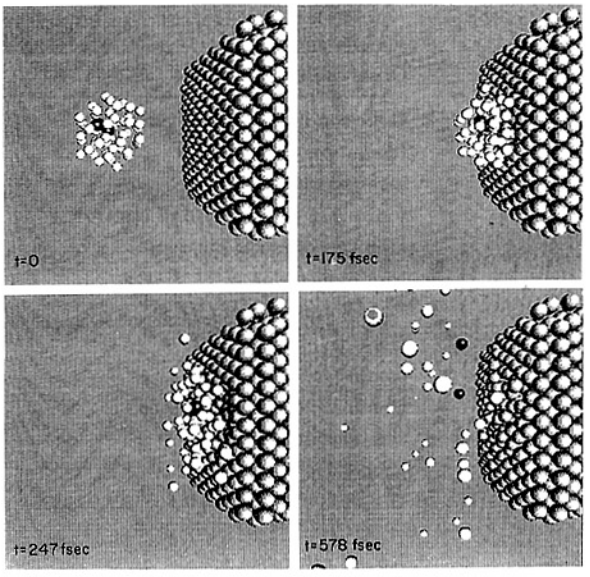

Fig. 13. Snapshots of the collision of a I_2Ar_{53} cluster with a Pt surface. The guest I_2 molecule (black balls) is located in an interior state within the Ar cluster (white balls). The Pt surface (grey spheres) consists of 6 layers, with 120 atoms each. The cluster temperature is 10 K and the surface temperature is 300 K. The times are marked on the four snapshots. At $t = 0$ the cluster with initial center-of-mass velocity $v = 10$ kmsec^{-1} ($E_k^0 = 1.23 \times 10^3$ eV) is located at a center-of-mass distance of 20 Å from the wall. At $t = 175$ fsec the cluster-wall impact achieves a peak of the cluster potential energy. Subsequently, cluster fragmentation occurs at $t = 247$ fsec, while at $t = 578$ fsec the dissociation of I_2 is clearly exhibited.

7. Dynamic Cluster-Size Effects

Continuing our excursion in the world of molecular clusters, we focus on dynamic cluster-size effects. An important class of dynamic phenomena pertains to specific-size effects on vibrational energy flow in molecular clusters, which exhibit a "transition" from reactive vibrational predissociation in small clusters (e.g., $Xe_2^*Ar_{11}$) to nonreactive vibrational relaxation in moderately large clusters (e.g., $Xe_2^*Ar_{54}$).[142] Another significant class of relaxation pertains to electronic–vibrational radiationless transitions,[178,179] which also exhibits specific size effects. We shall explore smooth dynamic cluster-size effects, which can be traced to cluster packing.

High-energy cluster–wall collisions[180–207] (with the acceleration of atomic or molecular cluster ions containing 10–500 constituents to velocities up to $v \sim 50$ kmsec^{-1} and kinetic energies up to $E_k^0 \sim 100$ keV) involve a novel high-energy, ultrafast, cluster-size-dependent energy-acquisition process.[181,203–206] When an internally cold, but rapidly moving, cluster collides with a relatively incompressible solid surface, a microscopic shock wave with an extremely high transient particle density (~ fourfold of the standard density), temperature (up to 10^6 K), and energy density (up to ~ 100 eV/particle) can be temporarily generated within the cluster on the fsec time scale, which constitutes a new medium, in which novel processes of energy acquisition and disposal are expected to occur. During the ultrashort time domain of the cluster–wall collision, thermal equilibrium is not ap-

proached, but rather energy may be localized, resulting in pair energies considerably exceeding the equilibrium energy.[203,205]

The energy-acquisition process for cluster-wall high-energy collision can be characterized by the residence time τ, which is given by the width (FWHM) of the time-dependent cluster potential-energy curve. τ provides the time scale for the prevalence of the intracluster microscopic shock wave. The cluster-size dependence of τ can be described in terms of a CSE, which can be traced to cluster packing. The residence time obeys the relation[181,203,205]

$$\tau = R_c/v\,, \tag{29}$$

where the cluster radius is given by Eq. (14), so that

$$[\tau(n)]^{-1} = (v/R_0)n^{-1/3}\,. \tag{30}$$

This dynamic CSE is borne out by molecular dynamics simulations for high-energy collisions between neat inert-gas clusters and a metal surface (Fig. 13).[203,205] This analysis of the v and size dependence of $\tau(n)$ (Fig. 14) provided a quantification of dynamic cluster-size effects.

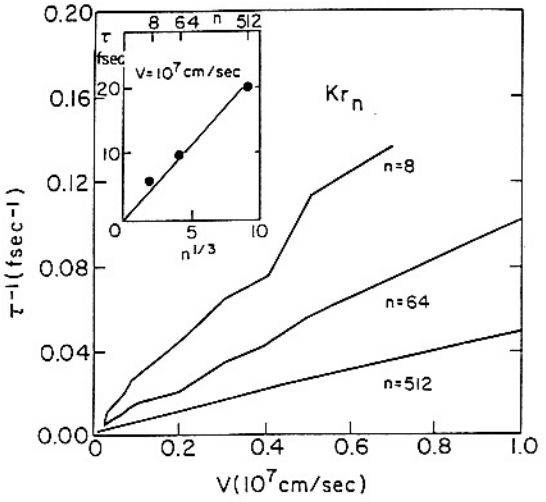

Fig. 14. The dependence of the inverse residence time of Kr_n clusters colliding with a Pt surface on the initial cluster velocity, according to Eq. (30). The insert shows the linear dependence of τ vs $n^{1/3}$ at a fixed cluster velocity $v = 10^7$ cmsec^{-1} ($E_k^0/n = 43$ eV).

8. Towards Cluster-Impact Chemistry

High-energy cluster-wall collisions provide a novel, unique, medium for the initiation and control of chemical reactions under extreme conditions of local desity, energy density, and temperature on the fsec time scale.[203,205,206] We have initiated theoretical[205,206] and experimental[207] studies on chemical reactions induced by cluster-ion high-energy collisions with surfaces. Many challenging questions arise, for example: (1) Can efficient conversion of cluster kinetic energy to intracluster energy be realized? (2) Can significant localization of internal energy occur within an impurity molecule embedded in the cluster and trigger a chemical reaction? (3) What is the cluster-size dependence of the yield of energy conversion and localization? (4) What is the cluster-velocity dependence of the yield of energy conversion and localization? (5) What are the mechanisms of the chemical reactions induced by cluster-wall collisions and do they differ from those induced by bare-molecule–surface collisions? (6) What are the time scales for energy acquisition, for energy localization and for a chemical reaction?

Our exploration of the new field of cluster-impact chemistry started with MD simulations of bond breaking of a diatomic molecule embedded in an atomic cluster, i.e., I_2 in rare-gas clusters, which collide (at the initial velocity v and kinetic energy E_k^0) with a metal Pt surface. The time scale τ for the energy acquisition for I_2Ar_n clusters is characterized by the cluster residence time, Eq. (29), with $R_c = R_0(n+\xi)^{1/3}$, where the numerical factor of $\xi = 2.9$ constitutes an I_2 self-volume correction. The linear plot of τ^{-1} vs v, according to Eq. (30), is well obeyed for $N = 11$–553 (Fig. 15). The slopes A of the linear relation $\tau^{-1} = Av$ are given by $A = R_0^{-1}(n+\xi)^{-1/3}$ (Fig. 15), with the reasonable value $R_0 = 2.5$ Å.

Of considerable interest are the I_2 dissociation yields Y_D,[205,206] which depend on the initial cluster kinetic energy E_k^0 and reveal a gradual increase of Y_D above threshold towards unity (Fig. 16). The initial kinetic-energy dependence of the dissociation yield of I_2 in I_2Ar_n or I_2Xe_n clusters quantitatively differs from the dissociation yield $Y_D(I_2)$ of bare I_2 on the Pt surface (Fig. 16).[205,206] $Y_D(I_2)$ vs E_k^0 reaches a shallow maximum and saturates at $Y_D = 0.35$. The

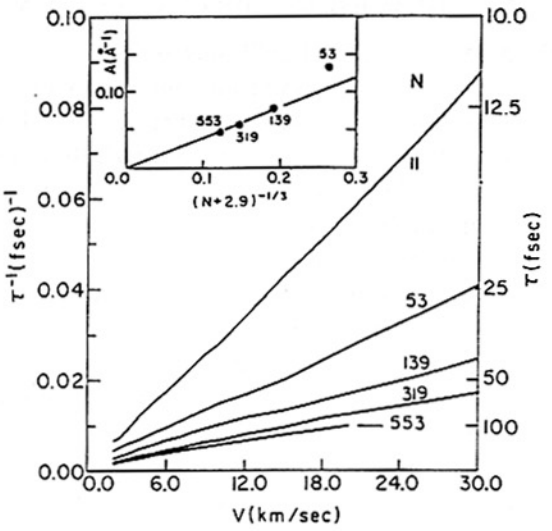

Fig. 15. The dependence of the inverse residence time of I_2Ar_n (n = 11, 53, 139, 319, and 553) clusters on the initial cluster velocity, according to Eq. (30). The slopes, A, of the linear plots $\tau^{-1} = Av$ obey the cluster dynamic size equation $A = R_0^{-1}(n + 2.9)^{-1/3}$ (with R_0 = 2.5 Å), as is evident from the insert.

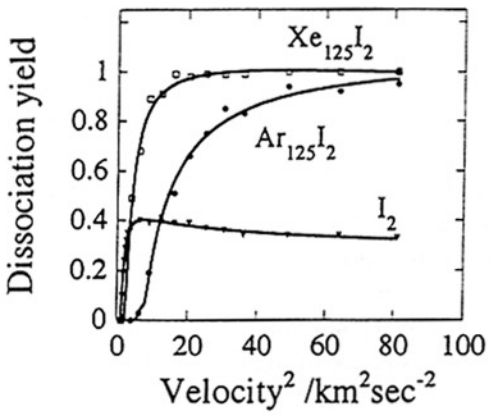

Fig. 16. The initial velocity dependence of the I_2 dissociation yields for the impact of bare I_2, I_2Ar_{125}, and I_2Xe_{125} clusters on a rigid Pt surface.

distinct kinetic-energy dependence of the dissociation yields of the bare I_2 and of the molecule in the cluster reveals novel features of cluster-impact dissociation dynamics.[205,206]. The dissociation mechanism of bare I_2 is dominated by a heterogeneous rotational excitation mechanism. On the other hand, the cluster-impact-induced dissociation of I_2Ar_n involves two parallel processes: (i) a heterogeneous dissociation mechanism on the surface; (ii) high-energy intracluster Ar–I_2 collisions, which result in vibrational excitation and dissociation of the guest. This homogeneous mechanism makes a marked contribution to the dissociation dynamics of I_2 rare-gas clusters.

Of considerable dynamic interest is the time scale for the cluster-impact-induced dissociation of the I_2 molecule. In our MD simulations[205,206] we have defined the origin of the time scale as the onset of the cluster-wall collision, and characterized the dissociation event by a geometrical criterion,[205] i.e., the attainment of the I–I distance of $1.34r_e$, where r_e = 2.66 Å is the equilibrium I–I separation. The mean dissociation times $\langle\tau_D\rangle$ in the impact-energy domain up to E_k^0/n = 30 eV reveal the following features: (a) for a given cluster, $\langle\tau_D\rangle$ decreases with increasing E_k^0; (b) for a fixed value of E_k^0/n, $\langle\tau_D\rangle$ increases with increasing the cluster size. The time scale for cluster dissociation at higher values of E_k^0/n (Fig. 17) is comparable to the vibrational time of the I_2 guest molecule, $\tau(I_2)$ = 156 fsec. Thus $\langle\tau_D\rangle \geq \tau(I_2)$ (Fig. 17), manifesting an ultrafast femtosecond chemical process on the time scale of the intramolecular motion. Cluster-impact dynamics opens up a new research area of thermal femtosecond chemistry.

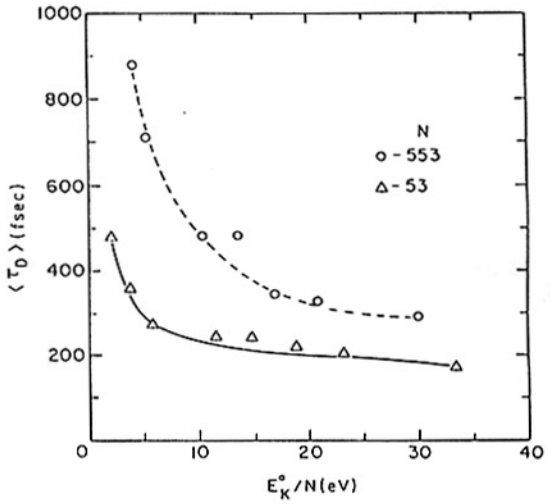

Fig. 17. The initial kinetic energy dependence (E_k^0/N) of the I_2 cluster Pt surface impact (averaged) dissociation times $\langle\tau_D\rangle$ of I_2 in I_2Ar_N clusters (N = 53 and 553). The two solid lines were passed through the data for N = 553 (top) and N = 53 (bottom) to demonstrate that $\langle\tau_D\rangle$ decreases with increasing E_k^0/n, and increases with increasing n. The shortest dissociation time scale for n = 53 at v = 10 kmsec^{-1} is $\langle\tau_D\rangle \simeq$ 150 fsec.

In 1977 at the ISSPIC-1 the exploration of the structure, energetics, spectroscopy, and dynamics of clean and isolated clusters constituted "a theoretician's dream".[1] This dream has come true.

Acknowledgments

We are grateful to Ori Cheshnovsky, Rina Giniger, Narda Ben-Horin, Neil R. Kestner, R. Bersohn, and U. Buck for stimulating and rewarding discussions. This research was supported, in part, by the German–Israeli Binational James Franck Program for laser–matter interaction (JJ, UE, and RDL). The support of the Z. Weinberg fund for research in chemical physics at Tel-Aviv University (JJ) is greatly appreciated. The Fritz Haber Center is supported by the Minerva Gesellschaft für die Forschung, mbH, Munich, Germany.

References

1. J. Friedel, *J. Phys. (Paris)* **C2**, 38, 1 (1977).
2. J. Jortner, *Ber. Bunsenges. Phys. Chem.* **88**, 188 (1984).
3. S. Bjørnholm, *Contemp. Phys.* **31**, 309 (1990).
4. Proceedings of the International Meeting on Small Particles and Inorganic Clusters, *J. Phys. (Paris)*, **C2**, 38 (1977).
5. Proceedings of the Second International Meeting on Small Particles and Inorganic Clusters, *Surf. Sci.* **106** (1981).
6. Proceedings of Bunsengesellschaft Discussion Meeting on Experiments on Clusters, *Ber. Gunsenges. Phys. Chem.* **88** (1984).
7. Proceedings of the Third International Meeting on Small Particles and Inorganic Clusters, *Surf. Sci.* **165** (1985).
8. *Metal Clusters*, eds. F. Träger and G. zu Putlitz (Springer, Berlin, Heidelberg, New York, 1986).
9. *The Physics and Chemistry of Small Clusters*, eds. P. Jena, B. K. Rao, and N. Khanna, NATO ASI Series (Plenum Press, New York, 1986).
10. *Microclusters*, eds. S. Sugano, Y. Nishima, and S. Onishi (Springer, Berlin, Heidelberg, New York, 1987).
11. *Large Finite Systems*, eds. J. Jortner, A. Pullman, and B. Pullman (Reidel, Dordrecht, 1987).
12. *Elemental and Molecular Clusters*, eds. G. Benedek, T. P. Martin, and G. Pacchioni (Springer, Berlin, Heidelberg, New York, 1988).
13. *The Chemical Physics of Atomic and Molecular Clusters*, ed. G. Scoles (North Holland, Amsterdam, 1990).
14. Proceedings of the Fourth International Symposium on Small Particles and Inorganic Clusters, *Z. Phys.* **D12** (1989).
15. Proceedings of the Fifth International Symposium on Small Particles and Inorganic Clusters, *Z. Phys.* **D19** (1990).
16. S. Sugano, *Microcluster Physics* (Springer–Verlag, Berlin, 1991).
17. Small Particles and Inorganic Clusters, *Z. Phys.* **D26** (1993).
18. *Physics and Chemistry of Finite Systems: From Clusters to Crystals*, eds. P. Jena, S. N. Khanna, and B. K. Rao (Kluwer, Dordrecht, 1992).
19. Proceedings of the Seventh International Symposium on Small Particles and Inorganic Clusters, this issue.
20. J. Gspann, in *Physics and Electronic and Atomic Collisions, Electronic and Atomic Impacts of Large Clusters* (North Holland, Amsterdam, 1982).
21. J. P. Toennies, in *The Chemical Physics of Molecular Clusters*, ed. G. Scoles (North Holland, Amsterdam, 1988) p. 597.
22. D. Brink and S. Stringari, *Z. Phys.* **D15**, 257 (1990).
23. S. Stringari, *Z. Phys.* **D20**, 219 (1991).
24. S. Stringari, in *The Chemical Physics of Atomic and Molecular Clusters*, ed. G. Scoles (North Holland, Amsterdam, 1990) p. 199.
25. B. P. Sindzingre, M. L. Klein, and D. Ceperly, *Phys. Rev. Lett.* **63**, 1601 (1989).
26. A. Scheidemann, J. P. Toennies, and J. A. Northby, *Phys. Rev. Lett.* **64**, 1899 (1990).
27. A Scheidmann, B. Schilling, and J. P. Toennies, *J. Phys. Chem.* **97**, 2128 (1993).
28. S. Goyal, G. N. Robinson, D. L. Schutt, and G. Scoles, *Phys. Rev. Lett.* **69**, 933 (1992).
29. J. Jortner, D. Scharf, and U. Landman, in *Excited-State Spectroscopy in Solids*, eds. V. Grassano and N. Terzi (North Holland, Amsterdam, 1987).
30. V. M. Nabutovskii and D. A. Romanov, *Sov. J. Low Temp.* **11**, 277 (1985).
31. M. Rosenblit and J. Jortner, *J. Chem. Phys.* **101**, 9982 (1994).
32. M. Rosenblit and J. Jortner, *J. Chem. Phys.* **101**, 8039 (1994).
33. Buddha (563–483 BC).
34. G. Mie, *Ann. Phys.* **25**, 377 (1908).
35. R. Kubo, *J. Phys. Soc. Jpn.* **17**, 975 (1962).
36. E. W. Becker, K. Bier, and W. Henkes, *Z. Phys.* **146**, 333 (1956).
37. E. W. Becker, R. Klingelhöfer, and P. Lohse, *Z. Naturforsch.* **17a**, 462 (1962).
38. J. Bauchert and O. F. Hagena, *Z. Naturforsch.* **20a**, 1135 (1965).
39. H. Burghoff and J. Gspann, *Z. Naturforsch.* **22a**, 684 (1967).
40. O. F. Hagena and W. Obert, *J. Chem. Phys.* **56**, 1793 (1971).

41. A. L. Mackay, *Acta Crystallogr.* **15**, 916 (1962).
42. M. R. Hoare, *Adv. Chem. Phys.* **40**, 49 (1969).
43. V. Hai and B. Vodar, *Z. Electrochem.* **64**, 756 (1960).
44. A. K. Kudian, H. L. Welshad, and A. Watanabe, *J. Chem. Phys.* **43**, 3397 (1965).
45. S. E. Novick, P. B. David, S. J. Harris, and W. Klemperer, *J. Chem. Phys.* **59**, 2273 (1973).
46. R. E. Smalley, D. H. Levy, and L. Wharton, *J. Chem. Phys.* **64**, 3266 (1974).
47. J. A. Beswick and J. Jortner, *Chem. Phys. Lett.* **49**, 13 (1977).
48. J. A. Beswick and J. Jortner, *J. Chem. Phys.* **68**, 2277 (1978).
49. R. Olinger, U. Schindewolf, A. Gaathon, and J. Jortner, *Ber. Bunsenges. Phys. Chem.* **75**, 690 (1971).
50. A. Gaathon, G. Czapski, and J. Jortner, *J. Chem. Phys.* **58**, 2648 (1973).
51. A. Gaathon and J. Jortner, *Can. J. Chem.* **55**, 1801 (1977).
52. H. Haberland, H.-G. Schindler, and D. R. Worsnop, *Ber. Bunsenges. Phys. Chem.* **88**, 270 (1984).
53. H. Haberland, H. Langosch, H.-G. Schindler, and D. R. Worsnop, *J. Phys. Chem.* **88**, 3903 (1984).
54. H. Haberland, C. Ludewigt, H.-G. Schindler, and D. R. Worsnop, *J. Chem. Phys.* **81**, 3742 (1984).
55. H. Haberland, C. Ludewigt, H.-G. Schindler, and D. R. Worsnop, *Surf. Sci.* **156**, 157 (1985).
56. J. V. Coe *et al.*, *J. Chem. Phys.* **92**, 3980 (1990).
57. G. H. Lee, *et al.*, *Z. Phys.* **D20**, 9 (1991).
58. J. Gspann, *Physica* **B169**, 519 (1991).
59. T. Jiang and J. A. Northby, *Phys. Rev. Lett.* **68**, 2620 (1992).
60. T. Jiang, S. Sun, and J. A. Northby, in *Physics and Chemistry of Finite Systems: From Clusters to Crystals*, ed. P. Jena (Kluwer Academic, The Netherlands, 1992) Vol. 1, p. 223.
61. T. Jiang, C. Kim, and J. A. Northby, *Phys. Rev. Lett.* **71**, 700 (1993).
62. E. C. Honea, M. L. Homer, P. Labastie, and R. L. Whetten, *Phys. Rev. Lett.* **63**, 394 (1989).
63. P. J. Campagnola, D. J. Lavrich, M. J. DeLuca, and M. A. Johnson, *J. Chem. Phys.* **94**, 5240 (1991).
64. I. V. Hertel, C. Huglin, C. Nitsch, and C. P. Schultz, *Phys. Rev. Lett.* **67**, 1767 (1991).
65. H. Haberland, T. Kolar, and T. Reiners, *Phys. Rev. Lett.* **63**, 1219 (1989).
66. P. R. Antoniewicz, G. T. Bennet, and J. C. Thompson, *J. Chem. Phys.* **77**, 4573 (1982).
67. J. L. Bellester and P. R. Antoniewicz, *J. Chem. Phys.* **85**, 5204 (1986).
68. G. Mo, C. C. Sung, and R. H. Richtie, *Chem. Phys. Lett.* **176**, 433 (1991).
69. P. Stampfli and K. H. Bennemann, *Phys. Rev. Lett.* **58**, 2635 (1987).
70. G. J. Martyna and B. J. Berne, *J. Chem. Phys.* **90**, 3744 (1989).
71. R. N. Barnett, U. Landman, C. L. Cleveland, and J. Jortner, *Phys. Rev. Lett.* **59**, 811 (1987).
72. R. N. Barnett, U. Landman, C. L. Cleveland, and J. Jortner, *J. Chem. Phys.* **88**, 4421, 4429 (1988).
73. R. N. Barnett, U. Landman, and J. Jortner, *Chem. Phys. Lett.* **145**, 382 (1988).
74. R. N. Barnett, U. Landman, N. R. Kestner, and J. Jortner, *J. Chem. Phys.* **88**, 6670 (1988).
75. R. N. Barnett, U. Landman, and A. Nitzan, *J. Chem. Phys.* **89**, 2242 (1988).
76. U. Landman, D. Scharf, and J. Jortner, *Phys. Rev. Lett.* **54**, 1860 (1985).
77. D. W. Heerman, *Computer Simulation Methods* (Springer, Berlin, Heidelberg, New York, 1986).
78. A. Rahman, *Phys. Rev.* **A136**, 405 (1964).
79. M. Parrinello and A. Rahman, *J. Chem. Phys.* **80**, 860 (1986).
80. B. J. Berne and D. Thirumalai, *Ann. Rev. Phys. Chem.* **37**, 401 (1986).
81. L. E. Fried and S. Mukamel, *Adv. Chem. Phys.* **26**, 217 (1993).
82. E. Neria, A. Nitzan, R. N. Barnett, and U. Landman, *Phys. Rev. Lett.* **67**, 1011 (1991).
83. W. Ekardt, *Phys. Rev.* **B29**, 1558 (1984).
84. W. Knight *et al.*, *Phys. Rev. Lett.* **52**, 2142 (1984).
85. W. de Heer, W. Knight, M. Chou, and M. L. Cohen, *Solid State Phys.* **40**, 93 (1986).
86. W. Pewerstorf, V. Bonacic-Koutecky, and J. Koutecky, *J. Chem. Phys.* **89**, 5794 (1988).
87. P. Pantucci, V. Bonacic-Koutecky, and J. Koutecky, *Z. Phys.* **D12**, 307 (1989).
88. J. E. Combariza, N. R. Kestner, and J. Jortner, *Chem. Phys. Lett.* **203**, 423 (1993).
89. J. E. Combariza, N. R. Kestner, and J. Jortner, *J. Chem. Phys.* **100**, 2851 (1994).
90. J. E. Combariza and N. R. Kestner, *J. Phys. Chem.* **98**, 3513 (1994).
91. J. E. Combariza, N. R. Kestner, and J. Jortner, *Chem. Phys. Lett.* **221**, 156 (1994).
92. R. Car and M. Parinelo, *Phys. Rev. Lett.* **55**, 2471 (1985).
93. G. Gali, R. M. Martin, R. Car, and M. Parinelo, *Science* **250**, 1547 (1990).
94. C. Bréchignac. Ph. Cahuzac, F. Carlier, M. de Frutos, R. N. Barnett, and U. Landman, *Phys. Rev. Lett.* **72**, 1636 (1994).
95. V. Bonacic-Koutecky, to be published.
96. R. D. Evans, *The Atomic Nucleus* (McGraw Hill, New York, 1955).
97. A. Bohr and B. R. Mottelson, *The Atomic Nucleus* (W. A. Benjamin, New York, 1969).
98. J. Farges, M. F. De Feraudy, B. Raoult, and G. Torchet, *J. Chem. Phys.* **78**, 5067 (1983).
99. J. Farges, M. F. De Feraudy, B. Raoult, and G. Torchet, *J. Chem. Phys.* **84**, 3491 (1986).
100. O. Echt, K. Sattler, and E. Recknagel, *Phys. Rev. Lett.* **47**, 1121 (1981).

101. O. Echt, O. Kandler, T. Leisner, W. Miehle, and E. Recknagel, *Faraday Symposium No. 25 on Large Gas Phase* Clusters (1989).
102. T. P. Martin, U. Näher, H. Schaber, and U. Zimmerman, *Phys. Rev. Lett.* **70**, 3079 (1993).
103. F. H. Stilinger and T. A. Weber, *Phys. Rev.* **A25**, 978 (1982).
104. F. H. Stilinger and T. A. Weber, *Phys. Rev.* **A28**, 2408 (1983).
105. A. Golberg, A. Heidenreich, and J. Jortner, *J. Phys. Chem.* **99**, 2662 (1995).
106. J. Jortner, E. E. Koch, and N. Schwentner, *Electronic Excitations in Condensed Rare Gases*, Springer Tract in Modern Physics 107 (Springer–Verlag, Heidelberg, 1985).
107. G. Baldini and R. S. Knox, *Phys. Rev. Lett.* **11**, 127 (1963).
108. G. Baldini, *Phys. Rev.* **137**, 508 (1965).
109. G. Gedanken, B. Raz, and J. Jortner, *J. Chem. Phys.* **58**, 1178 (1973).
110. D. Pudewill *et al.*, *Phys. Status Solidi* **74**, 485 (1976).
111. B. Raz and J. Jortner, *Proc. Roy. Soc.* **A317**, 113 (1970).
112. B. Raz and J. Jortner, *Chem. Phys. Lett.* **4**, 511 (1970).
113. I. Messing, B. Raz, and J. Jortner, *J. Chem. Phys.* **66**, 2239 (1977).
114. I. Messing, B. Raz, and J. Jortner, *J. Chem. Phys.* **66**, 4577 (1977).
115. I. Messing, B. Raz, and J. Jortner, *Chem. Phys.* **23**, 23 (1977).
116. S. Weber, S. A. Rice, and J. Jortner, *J. Chem. Phys.* **42**, 1907 (1965).
117. R. Kubo and Y. Toyozawa, *Prog. Theor. Phys.* **13**, 160 (1955).
118. M. Lax, *J. Chem. Phys.* **20**, 1752 (1952).
119. N. Ben-Horin, U. Even, J. Jortner, and S. Leutwyler, *J. Chem. Phys.* **97**, 5296 (1992).
120. N. Ben-Horin, U. Even, and J. Jortner, *J. Chem. Phys.* **97**, 5988, 6011 (1992).
121. R. Kubo, *Adv. Chem. Phys.* **15**, 101 (1969).
122. G. N. Robertson and J. Yarwood, *Chem. Phys.* **32**, 267 (1978).
123. W. G. Rotschild, J. Soussen-Jacob, J. Bessière, and J. Vincent-Geisse, *Chem. Phys.* **79**, 3002 (1983).
124. D. Thirumalai, E. J. Bruskin, and B. J. Berne, *J. Chem. Phys.* **83**, 230 (1985).
125. S. Mukamel, *J. Chem. Phys.* **77**, 173 (1982).
126. S. Mukamel, *Phys. Rep.* **93**, 1 (1982).
127. J. Sue, Y. J. Yan, and S. Mukamel, *J. Chem. Phys.* **85**, 462 (1986).
128. R. Islampour and S. Mukamel, *Chem. Phys. Lett.* **107**, 2391 (1984).
129. A. Heidenreich, D. Bahatt, N. Ben-Horin, U. Even and J. Jortner, *J. Chem. Phys.* **100**, 6300 (1994).
130. D. Bahatt, A. Heidenreich, N. Ben-Horin, U. Even, and J. Jortner, *J. Chem. Phys.* **100**, 6290 (1994).
131. A. Heidenreich and J. Jortner, *Isr. J. Chem.* **33**, 467 (1993).
132. A. Heidenreich and J. Jortner, *Z. Phys.* **D26**, 377 (1993).
133. L. E. Fried and S. Mukamel, *Phys. Rev. Lett.* **66**, 2340 (1991).
134. L. E. Fried and S. Mukamel, *J. Chem. Phys.* **96**, 116 (1992).
135. P. Parneix, F. G. Amar, and Ph. Bréchignac, *Z. Phys.* **D26**, 217 (1993).
136. T. Troxler and S. Leutwyler, *Ber. Bunsenges. Phys. Chem.* **96**, 1246 (1992).
137. T. Möller, *Z. Phys.* **D20**, 1 (1990).
138. J. Wörmer and T. Möller, *Z. Phys.* **D20**, 39 (1991).
139. M. Lengen, M. Joppien, R. Müller, J. Wörmer, and T. Möller, *Phys. Rev. Lett.* **68**, 2362 (1992).
140. M. Lengen, M. Joppien, R. von Pietorwski, and T. Möller, *Chem. Phys. Lett.* in press.
141. T. Möller, private communication and to be published.
142. D. Scharf, J. Jortner, and U. Landman, *J. Chem. Phys.* **88**, 4273 (1988).
143. J. Jortner, *Z. Phys.* **D24**, 247 (1992).
144. J. Jortner and N. Ben-Horin, *J. Chem. Phys.* **98**, 9346 (1993).
145. J. Jortner, *Zeitschr. Für Physikalische Chemie* **184**, 283 (1994).
146. J. Jortner, *J. Chim. Phys.* **92**, 205 (1995).
147. S. Stringari, *Phys. Lett.* **A107**, 36 (1985).
148. S. Stringari and J. Treiner, *J. Chem. Phys.* **87**, 5021 (1987).
149. D. S. Lewart, V. T. Pandharipande, and S. R. Pieper, *Phys. Rev.* **37**, 4950 (1988).
150. C. Bréchignac, Ph. Cahuzac, F. Carlier, F. M. de Frutos, and J. Leygnier, *Z. Phys.* **D19**, 1 (1991).
151. C. Bréchignac, Ph. Cahuzac, F. Carlier, F. M. de Frutos, and J. Leygnier, *J. Chem. Phys.* **93**, 7449 (1990).
152. G. Markovich, S. Pollack, R. Giniger, and O. Cheshnovsky, *Z. Phys.* **D26**, 98 (1993).
153. G. Markovich, R. Giniger, and O. Cheshnovsky, *J. Chem. Phys.* in press.
154. L. Perera and M. Berkowitz, *J. Chem. Phys.* **95**, 1954 (1991).
155. L. Perera and M. Berkowitz, *J. Chem. Phys.* **99**, 4222 (1993).
156. L. X. Dang and B. C. Garret, *J. Chem. Phys.* **99**, 2972 (1993).
157. J. Caldwell, L. X. Dang, and P. A. Kollman, *J. Am. Chem. Soc.* **112**, 9144 (1990).
158. L. X. Dang, J. E. Rice, J. Caldwell, and P. A. Kollman, *J. Am. Chem. Soc.* **113**, 2481 (1991).
159. J. Caldwell, L. X. Dang, and P. A. Kollman, *J. Am. Chem. Soc.* **112**, 9145 (1990).

160. L. X. Dang and D. E. Smith, *J. Chem. Phys.* **99**, 6950 (1993).
161. C. J. F. Böttcher, *The Theory of Electric Polarization* (Elsevier, Amsterdam, 1973).
162. L. E. Brus, *J. Chem. Phys.* **79**, 5566 (1983).
163. G. Makov and A. Nitzan, *J. Phys. Chem.* **98**, 3459 (1994).
164. I. Rips and J. Jortner, *J. Chem. Phys.* **97**, 536 (1992).
165. O. Cheshnovsky *et al.*, *J. Chim. Phys.* **92**, 397 (1995).
166. U. Even *et al.*, *Faraday Discuss. Chem. Soc.* **73**, 153 (1982).
167. S. Leutwyler and J. Jortner, *J. Phys. Chem.* **91**, 5558 (1987).
168. D. V. Brumbaugh, L. E. Kenny, and D. H. Levy, *J. Chem. Phys.* **78**, 3415 (1983).
169. T. A. Stephenson and S. A. Rice, *J. Chem. Phys.* **81**, 1083 (1984).
170. J. C. Alfano, S. J. Martinez, and D. H. Levy, *Chem. Soc. Faraday Trans.* **86**, 2503 (1990).
171. A. Heikal, L. Banares, D. H. Semmes, and A. H. Zewail, *Chem. Phys.* **156**, 231 (1991).
172. S. Leutwyler and J. Bösiger, *Chem. Rev.* **90**, 489 (1990).
173. A. Amirav, U. Even, and J. Jortner, *Chem. Phys. Lett.* **67**, 9 (1979).
174. A. Amirav, U. Even, and J. Jortner, *Chem. Phys.* **75**, 2489 (1981).
175. A. Penner, A. Amirav, J. Jortner, and A. Nitzan, *J. Chem. Phys.* **93**, 147 (1990).
176. C. Crepin and A. Tramer, *Chem. Phys. Lett.* **170**, 446 (1990).
177. U. Buck and R. Krohne, *Phys. Rev. Lett.* **73**, 947 (1994).
178. G. Gerber, *Z. Phys. Chem.* in press.
179. L. Wöste, private communication.
180. R. J. Beuhler and L. Friedman, *J. Mass Spectrom. Ion Phys.* **23**, 81 (1977).
181. L. Friedman and G. H. Vineyard, *Comments At. Mol. Phys.* **15**, 251 (1977).
182. R. Beuhler and L. Friedman, *Chem. Rev.* **86**, 521 (1986).
183. M. H. Shapiro and T. A. Tombrello, *Phys. Rev. Lett.* **65**, 92 (1990).
184. M. H. Shapiro and T. A. Tombrello, *Phys. Rev. Lett.* **68**, 1613 (1992).
185. J. F. Mahoney, J. Perel, T. D. Lee, P. A. Martino, and P. J. Williams, *Am. Soc. Mass Spectrom.* **3**, 311 (1992).
186. P. R. Wolfgang and R. Klingelhöfner, *J. de Physique* **C2**, 159 (1989).
187. V. I. Shulga, *Nucl. Instrum. Methods Phys. Res.* **B58**, 422 (1991).
188. H. Hsieh, R. S. Averbach, H. Sellers, and C. P. Flynn, *Phys. Rev.* **B45**, 4417 (1992).
189. H. Haberland, M. Karraris, M. Mall, and Y. Thurner, *J. Vac. Sci. Technol.* **A10**, 3266 (1992).
190. H. Haberland, Z. Insepov, and M. Moseler, *Z. Phys.* **D26**, 229 (1992).
191. I. Yamada, G. H. Takaoka, H. Usui, and S. K. Koh, *Mater. Res. Soc. Symp. Proc.* **206**, 383 (1991).
192. I. Yamada, *Appl. Surf. Sci.* **43**, 23 (1989).
193. Y. Yamamura, I. Yamada, and T. Tagaki, *Nucl. Instrum. Methods* **B37/38**, 902 (1987).
194. K. H. Müller, *J. Appl. Phys.* **61**, 2516 (1987).
195. H. P. Cheng and U. Landman, *J. Phys. Chem.* **98**, 3527 (1994).
196. P. M. St. John, R. D. Beck, and R. L. Whetten, *Phys. Rev. Lett.* **69**, 1467 (1992).
197. P. M. St. John and R. L. Whetten, *Chem. Phys. Lett.* **196**, 330 (1992).
198. R. D. Beck, P. M. St. John, M. M. Alvarez, F. Diederich, and R. L. Whetten, *J. Phys. Chem.* **95**, 8402 (1991).
199. C. Yeretzian and R. L. Whetten, *Z. Phys.* **D24**, 199 (1992).
200. C. Yeretzian, K. Hansen, and R. L. Whetten, *Science* **260**, 652 (1993).
201. U. Even, P. de Lange, H. Jonkman, and J. Kommandeur, *Phys. Rev. Lett.* **56**, 956 (1986).
202. K. Tögelhofer *et al.*, *Europhys. Lett.* **22**, 597 (1993).
203. U. Even, I. Schek, and J. Jortner, *Chem. Phys. Lett.* **202**, 303 (1993).
204. C. L. Cleveland and U. Landman, *Science* **257**, 355 (1992).
205. I. Schek, T. Raz, R. D. Levine, and J. Jortner, *J. Chem. Phys.* **101**, 8596 (1994).
206. T. Raz, I. Schek, M. Ben-Num, U. Even, R. D. Levine and J. Jortner, *J. Chem. Phys.* **101**, 8606 (1994).
207. U. Even and E. Hendell, to be published.